

# On the wall structure of the turbulent boundary layer

By R. F. BLACKWELDER AND R. E. KAPLAN

Department of Aerospace Engineering, University of Southern California,  
Los Angeles

(Received 8 April 1974 and in revised form 2 February 1976)

The wall structure of the turbulent boundary layer was examined using hot-wire rakes and conditional sampling techniques. Instantaneous velocity measurements indicate a high degree of coherence over a considerable area in the direction normal to the wall. At  $y^+ = 15$ , there is some evidence of large-scale correlation in the spanwise direction, but almost no indication of the streamwise streaks that exist in the lower regions of the boundary layer. Conditional sampling showed that the normal velocity is directed outwards in regions of strong streamwise-momentum deficit, and inwards when the streamwise velocity exceeds its mean value. The conditionally averaged Reynolds shear stress was approximately an order of magnitude greater than its conventionally averaged value and decayed slowly downstream.

---

## 1. Introduction

The existence of organized structures in the wall region of boundary-layer flows has been the subject of several experimental investigations. In the sublayer, an intermittent streamwise streaky structure was first observed by Hama (see Corrsin 1957) using dye injected at the wall. Bakewell & Lumley (1967) used an eigenfunction decomposition of space-time correlations in the sublayer and found that the velocity signals in this region could have been generated by pairs of counter-rotating vortices aligned in the streamwise direction. Using selective sampling techniques, Gupta, Laufer & Kaplan (1971) verified that the streamwise velocity was intermittently periodic in the spanwise direction.

In another visualization study, using hydrogen bubbles, Kline *et al.* (1967) observed the same intermittent streaky structure. They also found that occasionally one of these streaks of low streamwise momentum would lift away from the wall and interact with the outer flow field. This process was named ‘bursting’ because the interaction was quite sudden and a considerable amount of turbulence production occurred during this sequence. In a subsequent study, Kim, Kline & Reynolds (1971) state that “essentially all of the turbulent production occurs during bursting times in the zone  $0 < y^+ < 100$ ”. By observing the motion of neutrally buoyant particles in the wall region of a pipe flow, Corino & Brodkey (1969) came to the conclusion that the bursting phenomenon occurs approximately 18% of the time and accounts for 50–70% of the turbulence production.

The two-dimensional pressure pattern impressed upon the wall beneath a turbulent boundary layer was examined in a unique study by Emmerling (1973). He observed two-dimensional patterns of high amplitude pressure fluctuations which were convected downstream with convection velocities of  $0.4U_\infty$ – $0.8U_\infty$ . These patterns were highly correlated in both the spanwise and the streamwise direction with a length scale of approximately  $5\delta^*$  and could be followed downstream for at least one boundary-layer thickness.

Narahari Rao, Narasimha & Badri Narayanan (1971) used band-pass filtered hot-wire signals along with a detection criterion to study the frequency of occurrence of the bursts. Although they experienced some identification problems, their results indicated that the mean frequency of the velocity patterns which they observed scaled with the outer flow variables and not with the inner flow variables. This was also reported by Kim *et al.* (1971). In addition, Laufer & Badri Narayanan (1971) noted that the mean frequency of occurrence is approximately equal to the frequency of passage of the bulges in the outer turbulent/non-turbulent interface. In spite of the fact that the high Reynolds number data point used in the above frequency analysis is now doubtful (see Lu & Willmarth 1973*a*) these results still seem to indicate that the mean bursting frequency is a function of the outer flow variables. Thus, either the bursting phenomenon controls the development of the outer flow field by perhaps evolving into the large-scale structure characteristic of that region, or else the outer field determines the frequency of occurrence of the bursts. Both of these effects could be present through an intricate feedback mechanism.

Wallace, Eckelmann & Brodkey (1972), Lu & Willmarth (1973*b*) and Brodkey, Wallace & Eckelmann (1974) have studied this motion near the wall by using an instantaneous  $u, v$  signal. This signal was split into the four quadrants of the  $u, v$  plane, and the contribution to the tangential Reynolds stress  $\bar{uv}$  was obtained from each quadrant for various positions normal to the wall. Below  $y^+ \cong 15$ , the main contribution to the Reynolds stress was obtained from the fourth quadrant ( $u > 0, v < 0$ ), and above  $y^+ \cong 15$  the second quadrant ( $u < 0, v > 0$ ) provided the main contribution. Although this gives a broad categorization of the turbulent production, the lack of phase information eliminates the possibility of defining a coherent structure from the data.

Much less is known about the low momentum streamwise vortices in the sublayer. The previously cited research has determined that they have a characteristic spanwise wavelength of approximately  $z^+ = 100$ . However, the mean frequency of their intermittent occurrence is not known. In fact, it has not yet been determined how these vortices are initially formed. Are they the result of an inherent instability in the wall region, a feedback result of the bursting process itself or the result of still other unknown mechanisms?

Obviously, one would like to be able to understand these processes in the wall region better in order to predict and control bounded turbulent shear flows. If these processes can be assimilated into a deterministic analytical model (called a characteristic eddy) with the appropriate length and time scales, then the turbulent boundary layer could be described by a random distribution of these eddies having random amplitudes as discussed by Rice (1944) and Lumley

(1970, p. 80). Because of their intermittent nature, averages taken over long time periods will not disclose any details of these structures. Thus one must resort to conditional sampling techniques such as those used by Kaplan & Laufer (1969) and Kovasznay, Kibens & Blackwelder (1970). These techniques have been used in a Lagrangian frame to study the bursts by Grass (1971) and by some of the above-mentioned visualization studies as well. Conditional sampling of the bursting phenomenon in an Eulerian frame was first employed by Blackwelder & Kaplan (1972) and Willmarth & Lu (1972).

## 2. Equipment

### 2.1. *Wind tunnel*

The experiments were performed in the USC Low Turbulence Wind Tunnel, which has a speed range of from 8 to 40 ft/s. This tunnel is an open-return type in which the air enters a  $10 \times 10$  ft settling chamber, passes through four fine mesh screens, goes through a 16:1 contraction into the  $2 \times 3$  ft test section and exits through the fan to the atmosphere. The test section is 20 ft long and has an aerodynamically smooth wall, which was used for the flat plate. The boundary layer was tripped as it entered the test section, and the measurements were taken at a position approximately 17 ft downstream from the trip. At this position the Reynolds number based upon the momentum thickness varies from 2000 to 5800, depending upon the free-stream velocity. The side walls of the tunnel were flared slightly to ensure a zero pressure gradient in the test section. The downstream direction was denoted by  $x$ , the direction normal to the wall by  $y$  and the transverse direction by  $z$ . Most of the data were taken at  $R_\theta = 2550$ , which corresponded to  $\delta = 3$  in.,  $U_\infty = 15$  ft/s and  $u_* = 0.58$  ft/s.

### 2.2. *Hot-wire rakes*

A hot-wire rake was designed and built in order to observe the simultaneous variation of the streamwise velocity in the direction normal to the flat plate. The probe, shown in figure 1 (plate 1), was constructed on a  $1\frac{1}{2}$  in. Plexiglas plug which was mounted flush with the existing wall of the wind tunnel. The uprights were made of two  $0.010 \times \frac{3}{16}$  in. razor blades, which were glued onto the plug and extended  $\frac{1}{2}$  in. in the  $y$  direction above the flush surface. The space between the razor blades was open in order to minimize probe interference; however they were secured to each other at the outer extreme to improve the rigidity of the probe. The thick ends of jewellers broaches were cemented to the razor blades. These broaches extended upstream and were tapered to a diameter of 0.003 in. at the end. The tips of the broaches extended approximately 0.100 in. beyond the Plexiglas plug. Hot wires of 0.0001 in. diameter platinum were soft soldered onto the tips of the jewellers broaches. The ten hot wires were each 0.040 in. long and were located at distances of 0.022, 0.042, 0.065, 0.082, 0.120, 0.162, 0.200, 0.250, 0.300 and 0.403 in. from the wall. Electrical leads of 0.005 in. copper were attached at the rear of the uprights and passed through the Plexiglas plug to the exterior surface of the wind tunnel.

The Plexiglas plug was inserted into a hole on the centre-line of the 3 ft wide tunnel wall. The surface discontinuity between the plug and the wall was measured to be less than 0.0005 in., which is small compared with typical sublayer dimensions.

Another hot-wire rake was constructed in order to examine the instantaneous velocities in the spanwise ( $z$ ) direction. This probe, shown in figure 2 (plate 1), had a frame consisting of a  $\frac{1}{4}$  in. diameter stainless-steel tube (upper right-hand corner) aligned in the  $x$  direction. Two  $\frac{1}{8}$  in. diameter tubes 2 in. long extended towards the wall at an angle of  $45^\circ$ . These were attached to small uprights which held a  $0.010 \times \frac{3}{16} \times 1.30$  in. razor blade in the  $x, z$  plane. Twelve pairs of tapered jewellers broaches were cemented to the razor blade and extended upstream in the  $x$  direction approximately  $\frac{1}{4}$  in. Each pair of broaches was separated by 0.030 in. and tapered to 0.003 in. at the tip. Hot wires of 0.0001 in. diameter platinum were soft soldered to the jewellers broaches. The distance between the centre-lines of the twelve hot wires was 0.100 in.

The X-wires used in this experiment consisted of four tapered jewellers broaches extending  $\frac{1}{2}$  in. upstream from an epoxy streamlined body. When mounted, the 0.0001 in. platinum wires were 0.030 in. long and each was inclined at approximately  $45^\circ$  to the free-stream velocity vector. The spacing between the wires was approximately 0.015 in. The X-wires were always calibrated by rotation in the free stream prior to taking data.

A single hot wire sensitive to streamwise velocity fluctuations was often located at  $y^+ = 15$  and was used as a detector probe for the bursts. Two different configurations were used depending upon the data being recorded. For most measurements the single-wire probe protruded through a  $\frac{3}{16}$  in. hole in the wall. The hot wire was mounted on 0.003 in. tapered jewellers broaches which were epoxied to a  $\frac{3}{16}$  in. diameter probe body. When mounted, the only protrusions into the flow field were the tips of the broaches and the hot wire itself. All wake effects due to this probe had disappeared 0.090 in. downstream at the velocities used in this research.

The limited amount of movement of the above detector probe made it undesirable for use when recording data from the wall plug, which was by necessity fixed in space. Hence another probe was constructed, in a Y shape. Two 3 in. needles formed the arms of the Y and were epoxied onto a probe body. The tips of the needles were separated by roughly 3 in. Unetched 0.0002 in. platinum-rhodium Wollaston wire was soldered onto the needles and a 0.060 in. portion was etched in the middle between the tips of the two needles. According to the results of Champagne, Harris & Corrsin (1970) the wake effect of this wire should have been negligible 1 in. downstream.

### 2.3. *Hot-wire anemometers and associated electronics*

All of the hot wires were operated at a constant temperature with an overheat ratio of approximately 100%. The frequency response of the anemometers was flat over the range d.c. to 30 kHz. In order to obtain the highest possible signal-to-noise ratio, the outputs of each anemometer entered a bucking amplifier

which subtracted a fixed voltage and amplified the remaining signal by ten. These signals were then recorded on a fourteen-channel Hewlett Packard model 3955A FM magnetic tape recorder. A recording speed of 15 in./s was used, which provided a frequency response of d.c. to 5 kHz. The overall signal-to-noise ratio was approximately 70 dB.

In addition to the hot-wire output, the output signal from an MKS Baratron pressure transducer was recorded in order to monitor the free-stream velocity as obtained from the pressure difference from a Pitot-static tube. When using an X-wire, a signal proportional to the angle of inclination of the probe was recorded on the tape for calibration purposes.

The analog tape was played back on an identical Hewlett-Packard 3955A tape recorder located in the USC Engineering Computer Laboratory. Both calibration signals and data were digitized and processed on a digital computer. During the course of the data reduction, the hardware which performed the analog-to-digital conversions was changed from a 14 bit 10 V full-scale apparatus to one which gave a 12 bit 5 V full conversion. The loss of one bit in the conversions was not detectable in the experimental results. Digitized data were stored on either 9-track digital magnetic tape or digital disc bulk storage media for processing by simple FORTRAN programs. The techniques used are well known and will not be reported here.

### 3. Experimental procedure

#### 3.1. Calibration of hot wires

Whenever feasible, the hot wires were calibrated in the free stream of the wind tunnel. This was accomplished by operating the wind tunnel at several different velocities covering the range of velocities which the hot wires would experience in the boundary layer. The calibration technique had to determine the two constants in the familiar King's law plus an additional constant due to the unknown bucking voltage and amplification factors in the recording and playback amplifiers, etc. Thus a minimum of three velocities had to be used to determine the three constants. Since the velocities used in the calibration were known, the digitized data were used to obtain a least-squares fit for the unknown constants.

A similar procedure was followed for the X-wires, except that additional calibration points had to be used in order to determine correctly the angular dependence of these probes.

The wall plug and the detector probe protruding through the wall could not be placed in the free stream for calibration. Thus the velocity profile in the wall region was carefully measured by a single calibrated hot-wire probe for several values of the free-stream velocity. Then, by a least-squares fit, the mean velocity at any position in the wall region could be determined for several values of the free-stream velocity. With this information, calibration data from the wall probes were recorded *in situ* over a suitable time period and the recorded mean values were used to determine the necessary constants.

After obtaining the required constants as described above, the data were then

linearized using King's law for the  $u$ -sensitive hot wires. For the X-wires, King's law and a differencing technique based upon a generalized version of the cosine law of cooling were used to linearize the data and obtain the  $u$  and  $v$  velocity components. While it is recognized that such assumptions are not exact, the errors introduced were negligible over the range of velocities and flow angles which occurred, and the computations required were greatly simplified.

### 3.2. Detection criteria

While it is relatively straightforward to decide on a criterion for the presence of turbulence in the outer portion of the turbulent boundary layer, the detection of the bursting phenomenon near the wall is more difficult. Since the results of the visualization studies had indicated that the bursts were associated with a high degree of velocity fluctuation, a detection algorithm was designed to look for this condition. The guiding philosophy was to try to keep the criteria as simple as possible while yet retaining the essential features of the burst. In practice, this meant using a single hot wire, thereby concentrating on only the  $u$  fluctuations, and keeping the number of conditions (i.e. the number of IF statements) to a minimum.

In order to concentrate on a localized region in space (or time using Taylor's hypothesis) the variable-interval time-averaging (VITA) technique was employed. For a fluctuating quantity  $Q(x_i, t)$  the variable-interval time average is defined by

$$\hat{Q}(x_i, t, T) = \frac{1}{T} \int_{t-\frac{1}{2}T}^{t+\frac{1}{2}T} Q(x_i, s) ds, \quad (1)$$

where  $T$  is the averaging time. As  $T$  becomes large, the conventional time averaging results, i.e.

$$\bar{Q}(x_i) = \lim_{T \rightarrow \infty} \hat{Q}(x_i, t, T), \quad (2)$$

which is independent of  $t$  because of stationarity. In order to obtain a local average of some phenomenon, the averaging time  $T$  must be of the order of the time scale of the phenomenon under study. It may readily be seen that the VITA technique is a low-pass filter with  $1/T$  representing the cut-off frequency and gives a localized temporal measure of the quantity  $Q$ .

A localized measure of the turbulent energy is obtained by applying the VITA technique to the square of the streamwise velocity and subtracting the localized squared mean value. This is called the localized variance and is defined by

$$\widehat{\text{var}}(x_i, t, T) = \widehat{u^2}(x_i, t, T) - [\widehat{u}(x_i, t, T)]^2, \quad (3)$$

which is a positive-definite quantity. A typical example of the streamwise velocity at  $y^+ = 15$  and its associated variance signal is shown in figure 3. The detection criterion is completed by using a threshold level on the VITA variance signal. Thus the detection function  $D(t)$  is defined as

$$D(t) = \begin{cases} 1 & \text{if } \widehat{\text{var}} > k \cdot u_{r.m.s.}^2, \\ 0 & \text{otherwise,} \end{cases} \quad (4)$$

where  $k$  is the threshold level and  $u_{r.m.s.}$  is the root mean square of the total

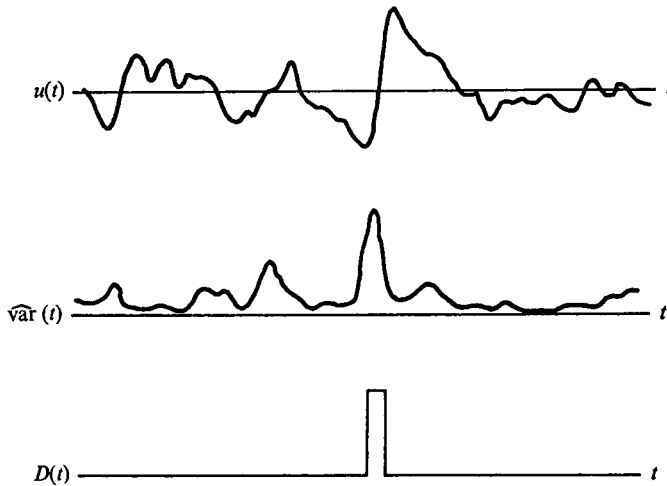


FIGURE 3. Schematic diagram of the detection process.

record of the signal, i.e.

$$u_{r.m.s.}^2 = \lim_{T \rightarrow \infty} \widehat{\text{var}}. \tag{5}$$

The application of this technique is described in §4 and the appendix explains how the conditional averages can be made independent of the threshold parameter,  $k$ .

### 3.3. Conditional averages

Once a reference time for each burst has been determined by the detection function, it is possible to study the bursting phenomenon in time and space by using conditional averaging techniques. The conditional average of a quantity  $Q$  is defined by

$$\langle Q(x_i, \tau) \rangle_{y^+} = \frac{1}{N} \sum_{j=1}^N Q(x_i, t_j + \tau), \tag{6}$$

where the independent variable  $x_i$  denotes the position in space at which the sampling occurred and the subscript  $y^+$  denotes the position at which detection occurred. The quantities  $t_j$  are those points in time when detection occurred. Since  $D(t)$  was equal to unity only during very short time intervals, the times  $t_j$  were taken to be midway between the beginning and end of the period during which  $D(t) \neq 0$ . A positive or negative time delay  $\tau$  was used to determine the temporal behaviour of  $Q$  before or after detection occurred, and  $N$  is the total number of samples added in the ensemble average.

### 3.4. Validity of the criterion

To test whether the conditional-sampling concept can yield information about the structure of turbulence, a ‘pseudo-turbulence’ signal was generated from a doubly exponentially filtered digital random-number generator. This corresponded to passing random noise through two first-order low-pass filters. When

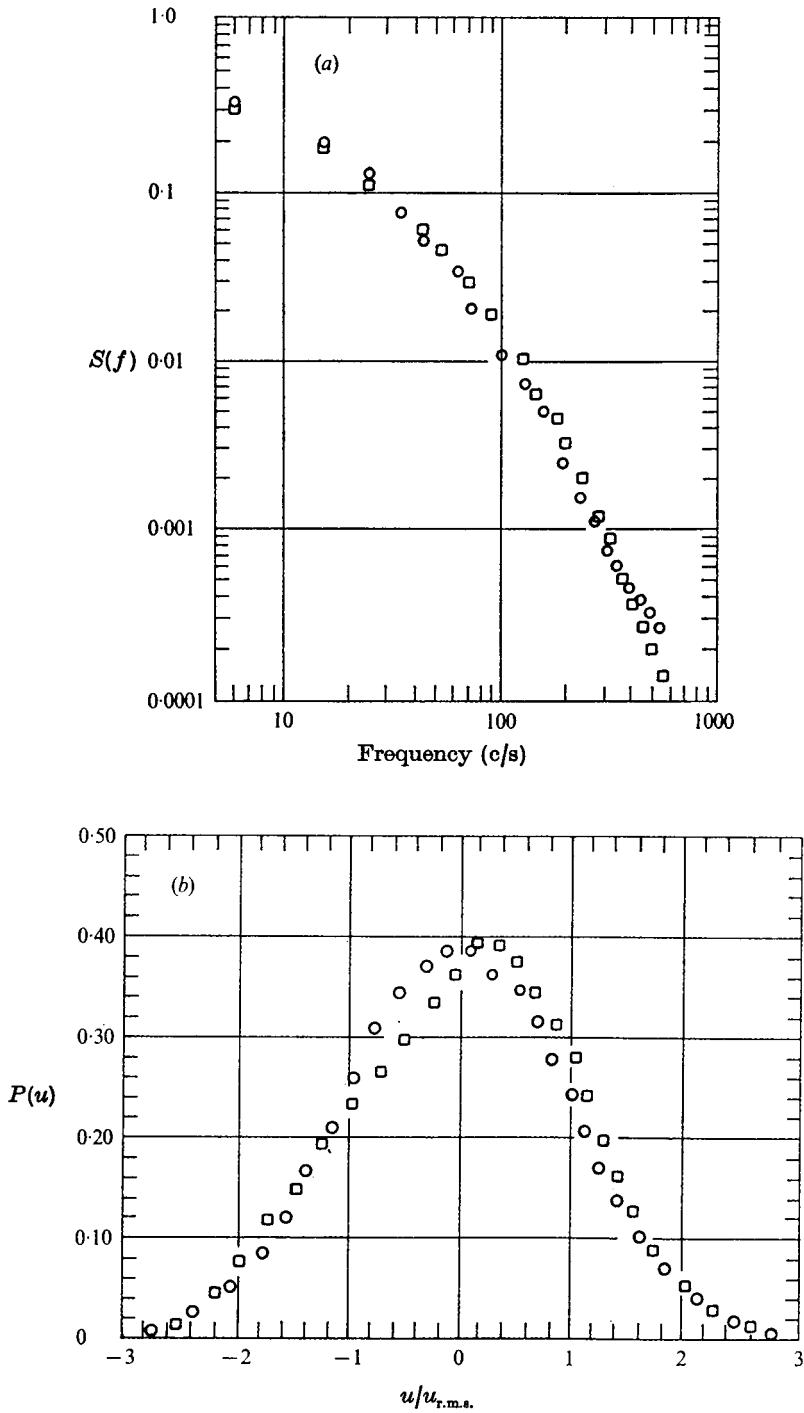


FIGURE 4. (a) Spectrum and (b) probability density function of pseudo-turbulence (circles) and boundary-layer turbulence at  $y^+ = 15, R_\theta = 2550$  (squares).

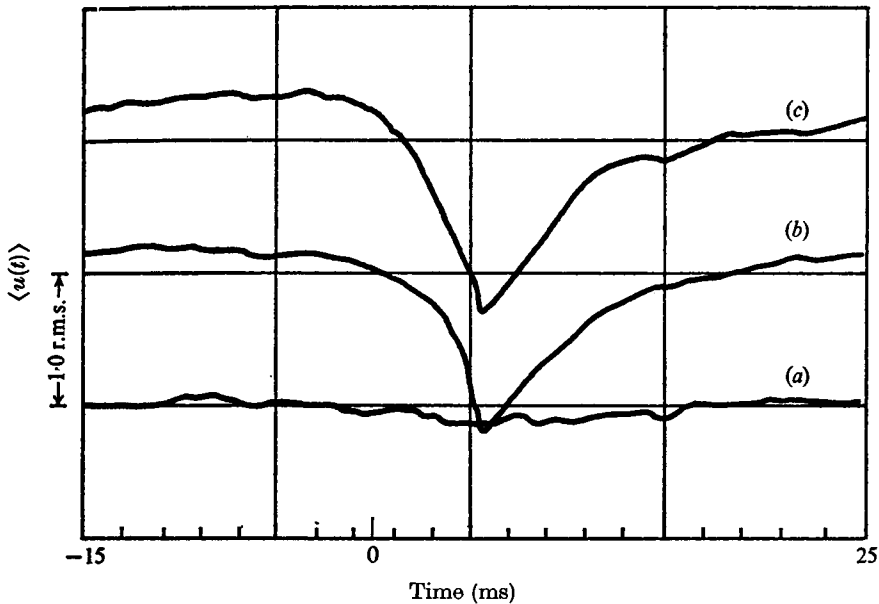


FIGURE 5. Conditional averages of pseudo-turbulence. (a) Detection by (4). (b) Detection if  $u < u_{r.m.s.}$ . (c) Detection if  $u < u_{r.m.s.}$  and  $du/dt < 0$ .

the spectrum of this signal was compared with that of the streamwise velocity at  $y^+ = 15$  the spectral differences were indeed small, as seen in figure 4(a). Although the original computer-generated noise had a uniform probability distribution, the filtered noise had a probability distribution that was similar to that of the experimentally measured turbulence (figure 4b).

When the detection criterion (4) was applied to the pseudo-turbulence and conditional averages were generated as defined in (6), there was barely a detectable departure from the time-averaged mean value, as shown in figure 5. However, different criteria based respectively on a level and on a level and a slope yielded substantially non-zero conditional averages.

In figure 5, the three traces represent the results of three different detection schemes. Trace (a) is that of (4), while for trace (b) a reference time was generated when the signal itself exceeded a large reference threshold and trace (c) had the added condition that the time derivative of the signal had a fixed sign. In both of these latter traces, the reference level and slope were negative, with the level set at 1 r.m.s. below the mean (which was zero for the pseudo-turbulence).

While this comparison does not invalidate the conclusions of a level-slope detection criterion, the similarity between the conditional averages shown in figure 5 for the pseudo-turbulence and those of Willmarth & Lu (1972) leads one to suspect that results derived using such a detection criterion may be more closely related to properties of the detector than to properties of the turbulence. In contrast, the detection based on (4) does not yield a similar bias for the pseudo-turbulence. The lack of a conditional average for the pseudo-turbulence leads one to expect that any conditionally averaged results for real turbulence are closely related to the turbulent structure, and not to the detection criteria.

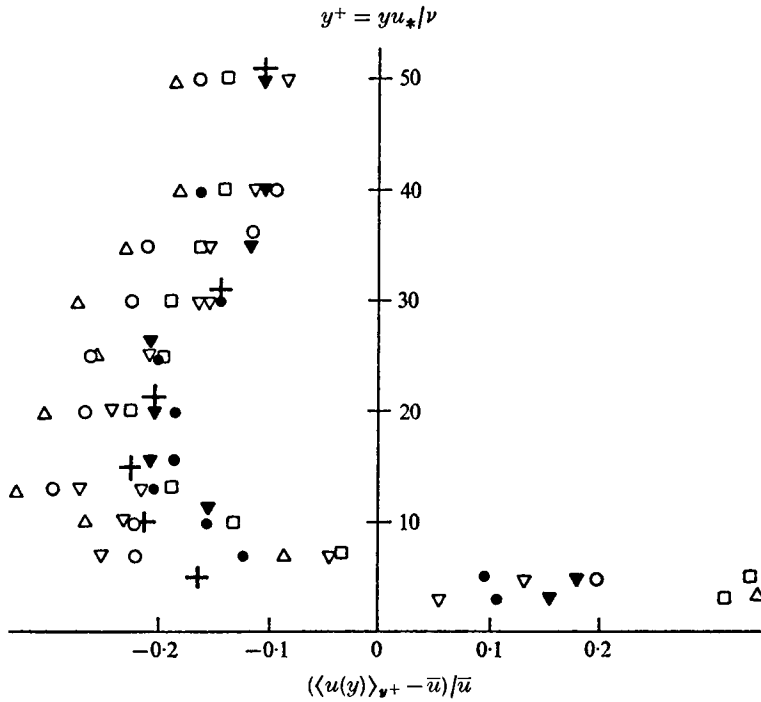


FIGURE 6. Conditional average of the streamwise velocity with triggering and averaging occurring at the same location.

It should be stressed that Willmarth & Lu did not sample their detector probe, but sampled velocities at adjacent positions. In view of the substantial spatial coherence (for example as shown in figure 8), the actual separation of the two probes does not substantially modify the arguments given above.

Additional comparative work was performed by Offen & Kline (1973) which attempted to compare local conditional sampling techniques (principally those described herein and those of Willmarth & Lu) with visual observations. Unfortunately, in an attempt to match the number of events visible in their field of view with that detected by the various criteria, they used a threshold significantly lower than that used in this study and, hence, did not observe a close correlation between their observations of bursting times and the detection by the various criteria.

## 4. Results

### 4.1. Detection

Initially, the hot wire was traversed across the boundary layer and the detection and sampling occurred simultaneously at the same location, which is indicated by the notation  $\langle u(y) \rangle_{y^+}$ . An example of the results of this type of averaging is shown in figure 6. The points summarize two Reynolds numbers (2500 and 5500, based on momentum thickness), three sets of decision times varying by a factor of two, and a set of thresholds varying by a factor of two. There was a trend that was evident as the decision time  $T$  and discriminator level  $k$  were changed.

Although the averages were not a strong function of the decision time  $T$ , it was observed that shorter times generated stronger defects. Higher discriminator levels had the same effect and are discussed more fully in the appendix.

It is readily observed that there is a non-trivial average substantially different from the time average when conditional sampling is used. Furthermore, spatial behaviour of the conditional averages was found to scale with the inner flow variables  $u_*$  and  $\nu$  and not with the outer variables  $U_\infty$  and  $\delta$ .

The results and the peak magnitude of approximately 25% of the local mean velocity are not very surprising, considering that these results agree with the observation that when the turbulent activity was high the velocities were low. There seems to be quite a distinct and easily detected relationship between a measure of the local intensity,  $\widehat{\text{var}}$ , and the local 'unsteady' mean velocity. These departures are all of the order of the conventional root mean square of the velocity and have to be regarded as an intensely strong effect.

Each data point is based on a set of approximately 100 samples detected during a 20 s run. The number of samples required to yield such consistent results also indicated that such a phenomenon is of basic importance to the dynamics of the buffer layer and sublayer. While not shown in the figure, these defects were still detectable out to  $y^+ = 500$ .

For  $y^+ < 100$  and  $k = 1.2$ , a typical value of the non-dimensional frequency, defined as  $f\delta/U_\infty$ , was approximately 0.13. In the outer interfacial region, the frequency  $f\delta/U_\infty$  is approximately 0.6 at the half-intermittency level according to Kovasznay *et al.* (1970). These two different values are not inconsistent with the idea that the parcels of turbulence ejected from the buffer layer may be associated with the bulges in the outer region in some intricate manner. The interface measurements include many crossings encountered on the edges of the large bulges. The turbulent bursts near the wall have a smaller size than the interfacial bulges, and the present measurements were able to centre more directly on a burst by varying the threshold level  $k$ . Thus one might expect a higher frequency in the outer region than near the wall.

For the remaining data reported herein, a threshold value of 1.2 and an averaging time of  $Tu_*^2/\nu \simeq 10$  were used. Since the largest effect on the conditional average in figure 4(a) is found at approximately  $y^+ = 15$ , that position was used for the location of the detector probe throughout the remainder of this study. It should be noted that Corino & Brodkey (1969) observed a low-speed region at this elevation just before a burst or ejection.

#### 4.2. Instantaneous streamwise velocity

After some preliminary data had been obtained and reported by Blackwelder & Kaplan (1972), it was readily apparent that it would be highly desirable to be able to examine and analyse simultaneous data in the normal and spanwise directions. An example of the simultaneous streamwise velocity signals as a function of the normal co-ordinate are shown in figure 7. The data shown were obtained at a Reynolds number based upon momentum thickness of 2550. The velocity fluctuations are not normalized, hence the larger fluctuations are most

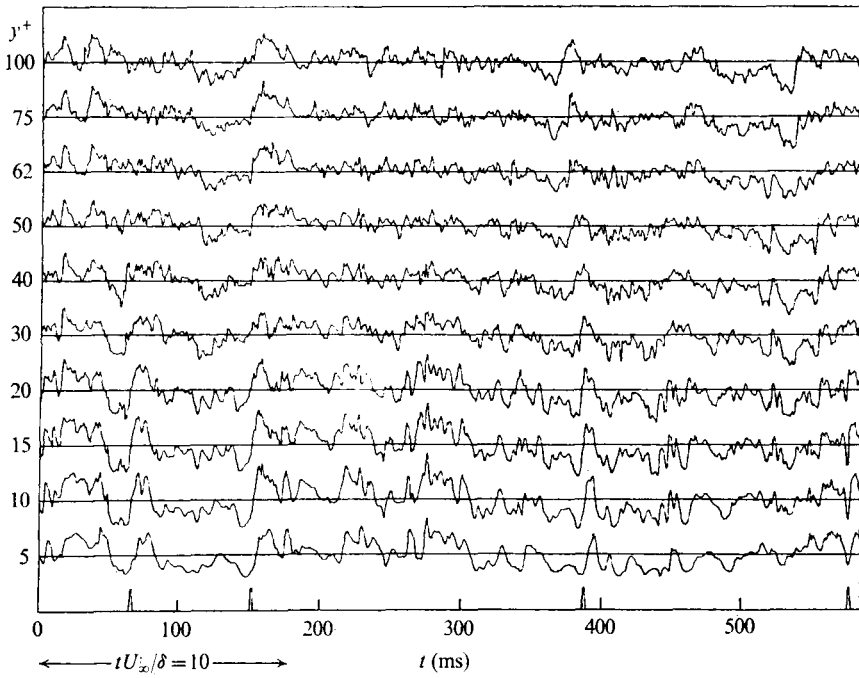


FIGURE 7. Instantaneous streamwise velocities as a function of the normal direction. The detector function obtained at  $y^+ = 15$  is shown between the tick marks.

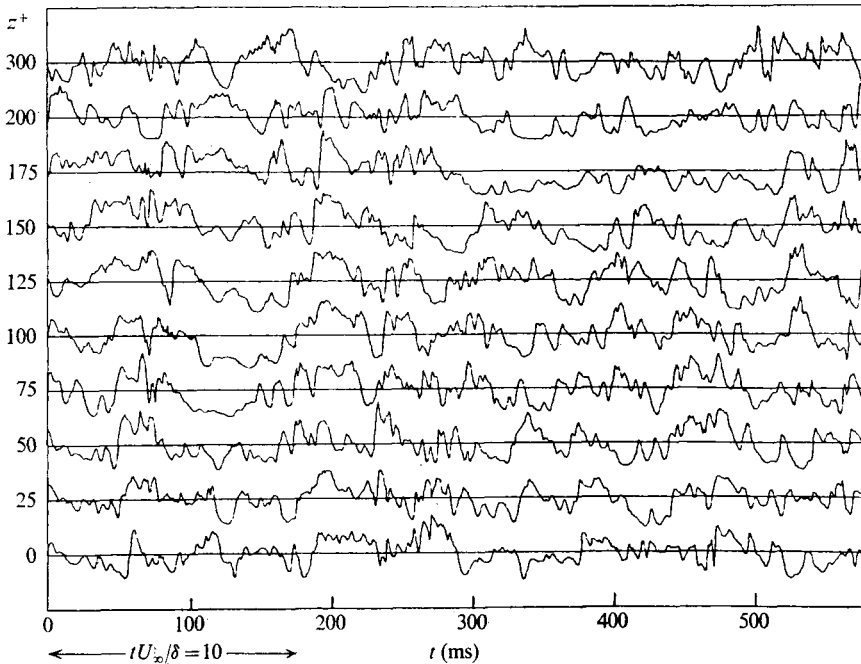


FIGURE 8. Simultaneous streamwise velocities in the spanwise direction;  $R_\theta = 2550$ ,  $y^+ = 15$ .

evident near the wall. Note that the time scale (streamwise dimension using Taylor's hypothesis) is grossly compressed compared with the normal dimension.

The detection criterion was applied to the signal at  $y^+ = 15$  and the points of detection are indicated on the time scale at the bottom of the figure. The detector function is highly correlated with the large streamwise velocity accelerations which are apparent in the lower regions of the boundary layer. This strong acceleration is associated with the large structure near the wall, and one can see a high degree of correlation throughout the entire wall region.

The data in figure 7 show that the bursts are not necessarily larger in amplitude than the background turbulence but are characterized by their high degree of coherence in time and in the direction normal to the wall. They are probably also characterized by their phase relationship with the streamwise velocity component, shown here, and the other velocity components.

The simultaneous streamwise velocities obtained with the probe shown in figure 2 are given in figure 8. The Reynolds number is the same as in figure 7 and the data were obtained at  $y^+ = 15$ . The large-scale correlation which was so evident in the normal direction is almost non-existent in the spanwise direction. One of the most striking features of these data is the existence of large regions containing small fluctuations. There is almost no evidence of the streaks which are found closer to the wall, however there are isolated regions where some degree of anticorrelation can be seen.

The strong accelerations can still be observed and show some correlation in the  $z$  direction. However, they are correlated over only small spanwise distances, which was substantiated by computing the detection signal for all ten signals and forming its autocorrelation. The results showed a very small spatial scale in the spanwise direction in agreement with Lu & Willmarth's (1973*b*) results. This is further evidence that the streaky structure observed in the lower regions by Gupta *et al.* (1971) is not as prevalent at  $y^+ = 15$ .

There is another interesting feature in the spanwise direction. When the strong acceleration is evident at two or more adjacent hot wires, there is usually a time delay between the two signals. Transforming this time delay into a spatial separation by using Taylor's hypothesis, it is found that the structure occupies a narrow region in the  $z$  direction. The sharp accelerations tend to be skewed at small angles to the mean velocity vector of approximately  $15^\circ$ – $25^\circ$ . From the symmetries imposed in the  $x, z$  plane, this angle must be equally probably on either side, even though the examples in figure 7 seem to have a preference for one direction.

#### 4.3. Conditional averages

The conditionally averaged velocity profiles are shown in figure 9 as functions of  $y^+$  and the time delay  $\tau$ . From (6), the time delay is with respect to the point of detection. Since the appropriate scaling for the time delay is not known, it is given in milliseconds. The dashed lines in the figure give the mean velocity profile obtained by conventional averaging, and the solid lines are the conditionally averaged profiles during the bursting phenomenon.

The first deviations from the mean profile occur approximately 17 ms before

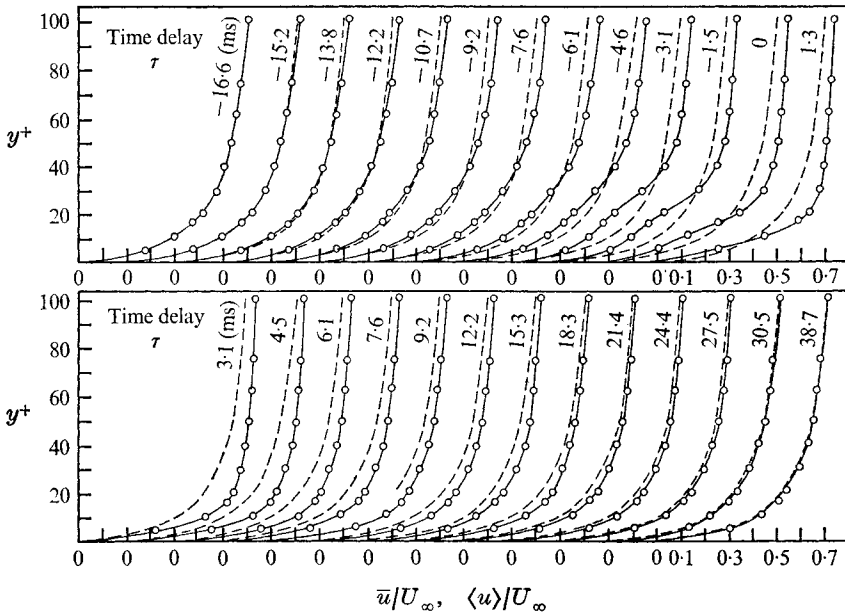


FIGURE 9. Conditionally averaged and mean velocity profiles with positive and negative time delay  $\tau$  relative to the point of detection. +,  $\bar{u}/U_\infty$ ;  $\circ$ ,  $\langle u \rangle/U_\infty$ .  $Re_\theta = 2550$ ,  $U_\infty = 14.0$  ft/s,  $u_x = 0.52$  ft/s.

the detection occurs, and the mean profile is not re-established until approximately 37 ms after detection. In the outer regions a momentum excess is evident throughout the entire sequence. In the early stage of the event, the fluid nearest the wall is retarded and a streamwise momentum defect continues to build up until  $\tau = 0$ . Directly before detection, the velocity deficit is greater than one r.m.s. value and an inflexional velocity profile is quite evident. Thereafter a strong momentum excess is evident throughout the entire region.

This sequence of events is the same as that reported by Kline *et al.* (1967) and Corino & Brodkey (1969), who also observed a strongly inflexional profile to be a characteristic feature of the bursts. However, it is still not clear whether the inflexional profile is the cause or result of the bursting phenomenon.

The data shown in figure 9 were averaged over approximately 300 bursts and represent a total time of  $TU_\infty/\delta = 2.8$ . The average frequency of occurrence was  $f\delta/U_\infty \approx 0.1$ . Although it is difficult to ascertain the beginning and end of the bursting cycle, the above two numbers indicate that the bursting process occupies approximately 25% of the total time at this Reynolds number.

Conditional averages were taken over longer periods of time as well. The only deviations from the mean profile occurred in the outer regions, where there was always a very small momentum defect.

The data shown in figure 9 are replotted in figure 10 for a longer time delay. In this figure the mean values of the velocity have been subtracted and all values are normalized with the r.m.s. velocity at the corresponding  $y$  location. Note that the strong accelerations which were found in the lower regions of the boundary layer in figure 7 are still evident in figure 10 and that the strongest accelerations

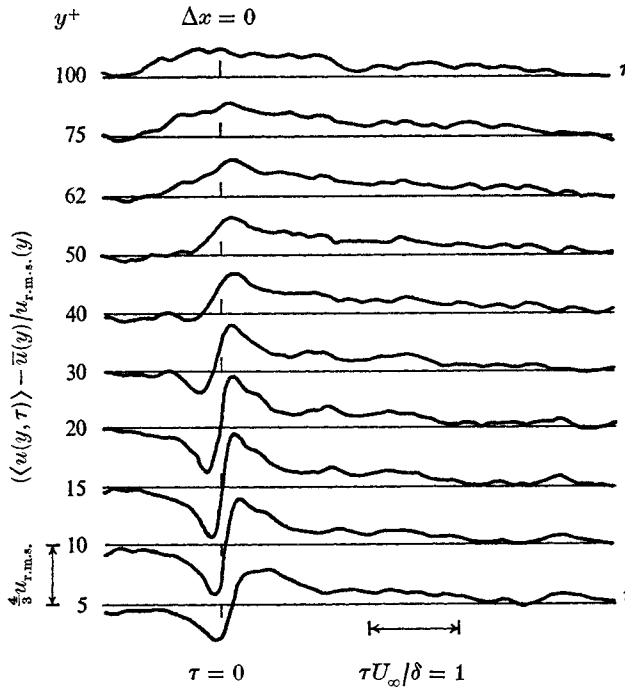


FIGURE 10. Conditionally averaged streamwise velocities at ten  $y^+$  locations. The detection criterion was applied at  $y^+ = 15$ .  $R_\theta = 2550$ .

occur at  $y^+ = 15-20$ . However, above that location the magnitude of the acceleration decreases and is completely lost at the higher values of  $y^+$ . This is expected because at larger  $y^+$  the large structure not only occurred earlier in time as is evident in figure 7, but also had a more random phase than in the wall region. That is, in the buffer layer and sublayer, the strong accelerations occur almost simultaneously and are highly correlated. However, above  $y^+ = 25$ , the occurrence of the strong acceleration and the large eddy structure is not only earlier in time, but its phase is more random than below  $y^+ = 25$ . Thus, by using the detection criterion at  $y^+ = 15$  and conditional sampling, one expects that the strong acceleration below  $y^+ = 25$  will be quite evident, whereas above  $y^+ = 25$  the random phase will tend to smooth out the acceleration as is evident in figure 10.

Even though there were approximately 300 time sequences contributing to the ensemble average shown in figure 10, there seem to be some slight oscillations, especially at the larger values of  $y^+$ . This was also evident in the data of Blackwelder & Kaplan (1972) and has been found in other investigators' data as well. This might mean that there is an oscillation of some preferred frequency associated with the bursting phenomenon, however the magnitude of the oscillation shown in figure 10 is too small to make any firm conclusions. This could also be a result of the random phase between detection applied at  $y^+ = 15$  and the acceleration occurring at  $y^+ = 100$ . It should be remembered that Kline *et al.* (1967) also suggested that there was some preferred oscillation associated with the bursting phenomenon.

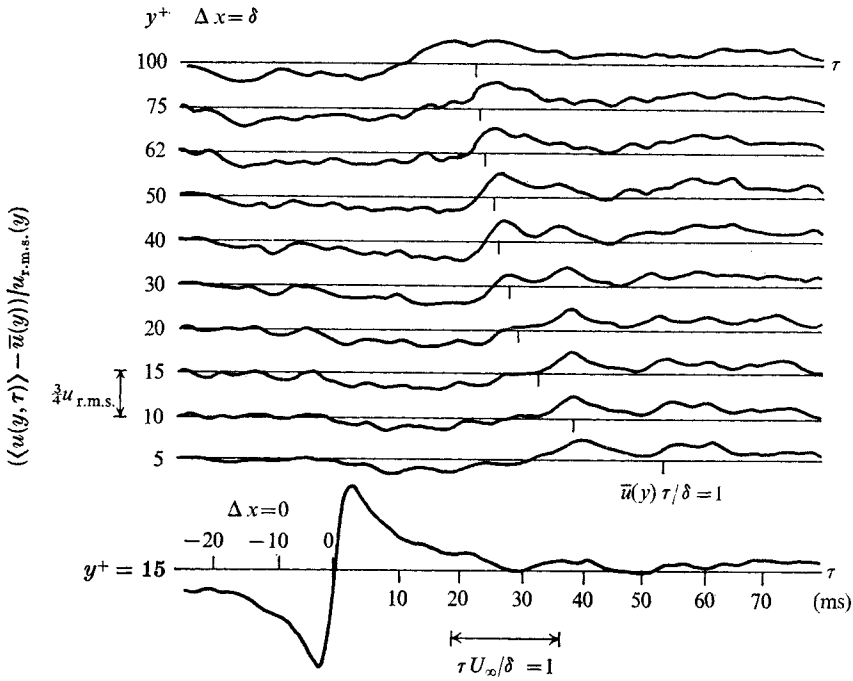


FIGURE 11. The conditionally averaged streamwise velocities obtained one boundary-layer thickness downstream from the point of detection of the burst.  $R_\theta = 2550$ .

Obviously, one would like to know how this structure decays as it is swept downstream. To achieve this goal an additional trigger wire was located one boundary-layer thickness upstream at  $y^+ = 15$ . The detection was generated from the velocity signal of the upstream probe and the downstream velocity profiles were then conditionally averaged with a time delay.

The results are shown in figure 11, which has the same format as figure 10. The magnitude of the conditionally averaged velocities is much smaller than with zero streamwise separation, as is expected. The pattern seems to have travelled one boundary-layer thickness downstream at a velocity much faster than the local mean velocity, especially in the lower regions. Using Taylor's hypothesis, the expected arrival time at each  $y^+$  position is indicated by the tick mark on the horizontal axis. It may be readily seen that at  $y^+ = 5$  the structure has arrived much earlier than it would have done had it been convected at the local mean velocity

Directly after the burst is detected upstream, there is a general velocity defect downstream at the location of the ten-wire probe. At later delay times a velocity excess occurs at all locations downstream, starting with the outermost position and moving towards the wall. This is consistent with the prior observation that the structure associated with the strong acceleration occurs earlier in the outer region of the boundary layer. However, the most interesting phenomenon exhibited here is not that an excess of momentum occurs, but rather the manner in which it manifests itself. In the lower regions, the velocity excess arrives quite

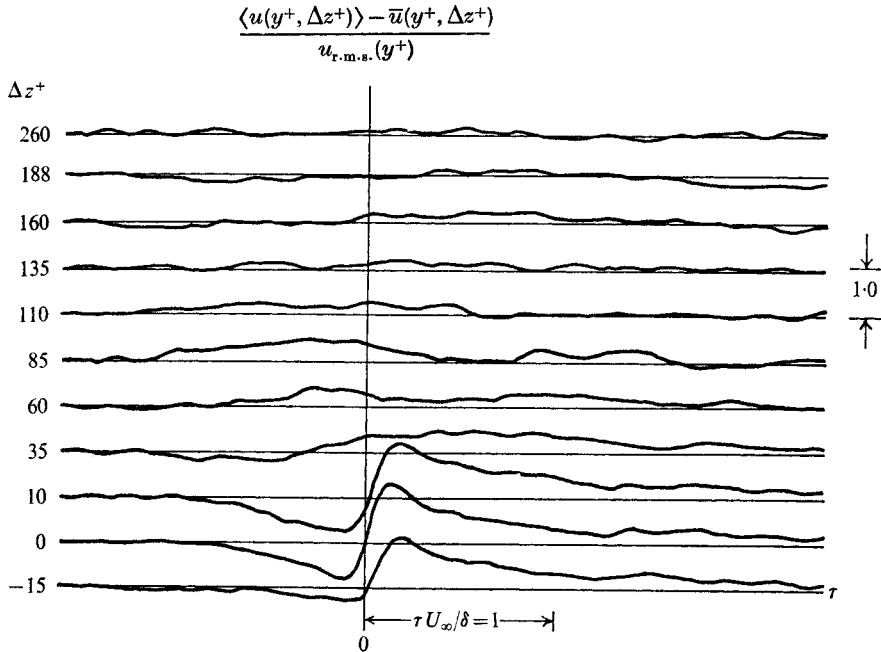


FIGURE 12. The conditionally averaged streamwise velocities as a function of the spanwise co-ordinate.  $R_\theta = 2550$ ,  $y^+ = 15$ ,  $\Delta x = 0$ .

early, and one can see the strong vertical correlation up to  $y^+ = 50$ . However, above  $y^+ = 20$ , a different phase of the velocity excess appears earlier in time and again has a strong vertical correlation seen across the whole region. One could speculate that another phase is starting to occur at  $y^+ = 100$ . The entire structure seems to have an oscillatory motion with its phase almost constant across the lower boundary layer. However this oscillatory structure appears earlier and earlier as one moves outwards from the wall. When individual members of the ensemble were studied, this oscillatory structure was quite dominant in some and almost lacking in others. This may possibly be due to a three-dimensional nature of the bursting phenomenon. That is, as the burst moves downstream, it may move at a skewed angle in a plane parallel to the wall, as indicated by the results shown in figure 8.

The conditionally averaged velocities in the spanwise direction are shown in figure 12. These data were obtained at  $y^+ = 15$  and at a Reynolds number of 2550. An additional detector wire was inserted through the wall and located at  $y^+ = 15$  and at  $\Delta z^+ = 0$ . There was no streamwise separation between the detector probe and the rake. The conditional average of the trigger wire is shown  $\Delta z^+ = 0$  and the strong streamwise acceleration is readily apparent. This streamwise acceleration is also evident in the region directly adjacent to the trigger probe at  $\Delta z^+ = -15$  and 10. It can be seen that the conditional averages indicate that this structure is not correlated over a very large spanwise distance. In fact, there seems to be very little evidence of the bursting structure beyond  $\Delta z^+ = 100$ .

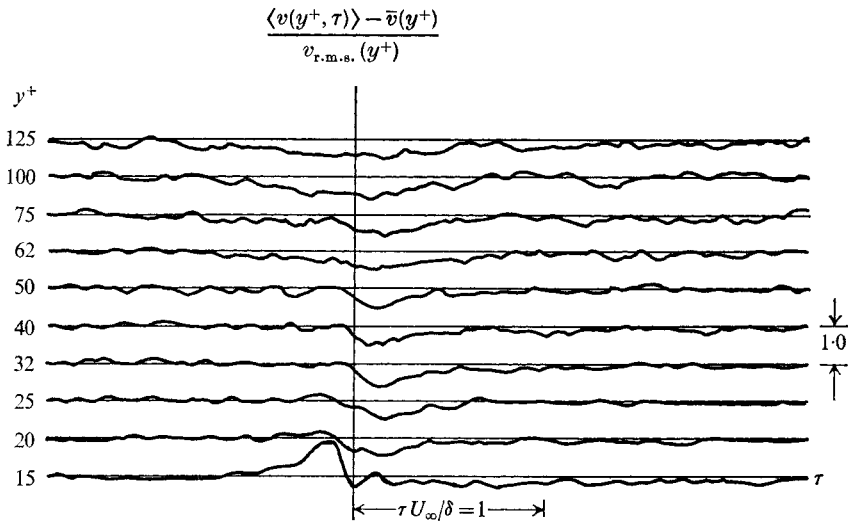


FIGURE 13. The conditionally averaged velocity component in the normal direction.  $R_\theta = 2550$ ,  $\Delta x = 0$ .

However, there is a broad momentum excess at  $\Delta z^+ = 60$  and  $85$ . The location of this broad momentum excess corresponds to an angle of roughly  $20^\circ$ – $30^\circ$  with respect to the mean velocity in the upstream direction from the trigger wire. Thus the preferred angles found in figure 8 also exist in the conditional averages. Obviously, from symmetry considerations, a similar broad momentum excess must occur in the  $-\Delta z^+$  direction as well.

Note that the positive momentum excess at  $\Delta z^+ = 60$  and  $85$  arrives earlier in time than the strong streamwise acceleration at  $\Delta z^+ = 0$ . Thus this structure may either be skewed slightly from the streamwise direction, with equal probability to each side, or may possibly be V-shaped.

Another interesting aspect of these conditional averages is that at  $\Delta z^+ = 50$ – $100$  the averages are almost always greater than zero, whereas the raw data in figure 8 indicate that one might expect to see some remnants of the sharp acceleration. However, at  $\Delta z^+ = 0$ , one can see that the average velocity excess during the bursting period is greater than the velocity defect. Thus, if this structure were skewed at a non-constant angle from the streamwise direction as indicated above, the net conditionally averaged result away from  $\Delta z^+ = 0$  would be positive. This problem will be discussed later.

The normal velocity component was conditionally averaged by positioning a trigger wire at  $y^+ = 15$  and traversing an X-wire above it. The results are shown in figure 13 for zero streamwise and spanwise separation. In general, there seems to be a broad movement of fluid towards the wall as evidenced by the negative values of the normal velocity component. A strong exception to this occurs at  $y^+ = 15$  directly before detection occurs. At this position there is a strong velocity away from the wall. This is associated with a deficit in the streamwise velocity component as seen earlier. Thus the low-speed streamwise

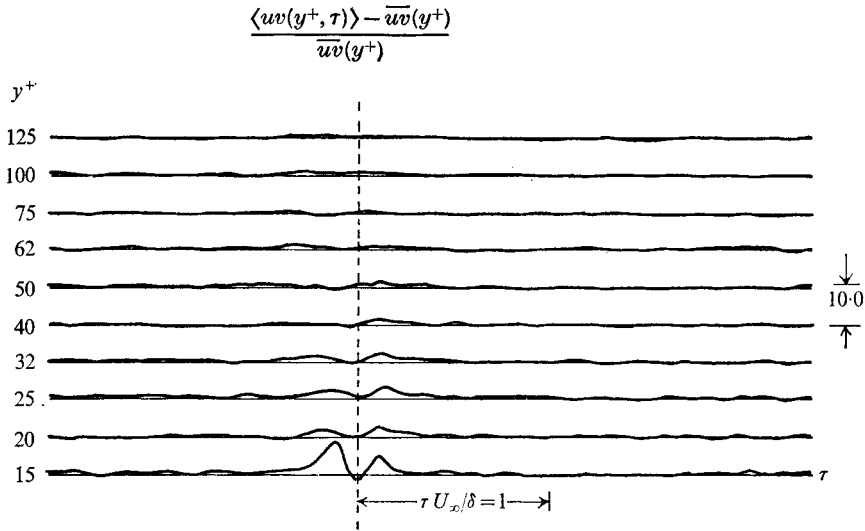


FIGURE 14. The conditional averages of the Reynolds shear stress at  $\Delta x = 0$ ,  $R_\theta = 2550$ .

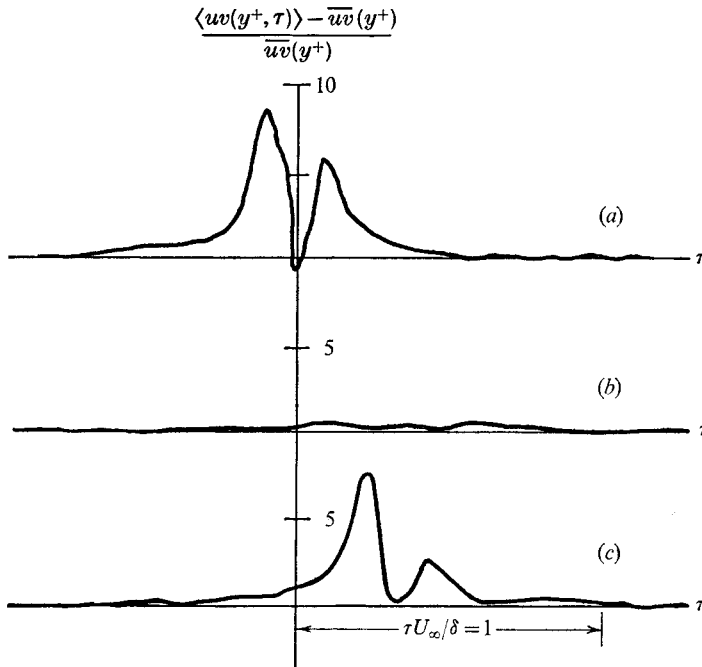


FIGURE 15. Conditional averages of the Reynolds shear stress at  $y^+ = 15$ . (a)  $\Delta x = 0$ , from figure 14. (b) Similar average taken one-quarter boundary-layer thickness downstream. (c) Also obtained one-quarter boundary-layer thickness downstream, after correcting for the random convection velocity.

momentum is being lifted away from the wall in this region, which agrees with the visual results of Kline *et al.* (1967) and Corino & Brodkey (1969).

The Reynolds shear stress was conditionally averaged in the same manner as the normal velocity component. The results are shown in figure 14. In the upper regions there is some excess Reynolds shear stress over and above the mean value. As one approaches the wall, this excess of Reynolds shear stress becomes much more predominant. In fact, at  $y^+ = 15$  the maximum conditionally averaged Reynolds shear stress is approximately nine times the mean value directly before the detection occurred. This is associated with a deficit of streamwise momentum and a normal velocity component away from the wall.

In an attempt to follow this structure downstream, the conditionally averaged Reynolds shear stress was also measured at  $\Delta x = \frac{1}{4}\delta$ , and is shown in figure 15. Curve (a) is the conditionally averaged Reynolds stress as shown for  $y^+ = 15$  in figure 14 and curve (b) is the same stress averaged downstream of the detection position. Note that the original strong excessive Reynolds shear stress has now almost completely disappeared. This was quite surprising, because if the bursting phenomenon was so important in the turbulence production process, then the Reynolds stress associated with this phenomenon should not die out so quickly downstream. At about the same time as this was discovered, Lu & Willmarth (1973*b*) also reported that they had found practically zero excess Reynolds stress at  $\Delta x = 2.5\delta^* \approx \frac{1}{4}\delta$  downstream.

After exploring several different explanations, it was determined that this effect is due to the randomness of the convection velocity. That is, the velocity associated with the bursting structure at  $y^+ = 15$  has both a strong momentum defect and a strong momentum excess. If different bursts travel downstream at slightly different convection velocities, this excess and this defect will tend to smear each other out, as was seen in figure 11. Since the Reynolds shear stress is strongly dependent upon the phase relationship between the streamwise and normal velocity components, any slight deviations in the convection velocity are bound to erase the strong positive Reynolds shear stress seen at  $\Delta x = 0$ .

In order to overcome this difficulty, the detection criterion was applied again at the downstream location. Then, if the time difference between detection at the upstream and downstream positions was within the possible limits established by the maximum and minimum values of the convection velocity, the Reynolds shear stress was conditionally averaged with respect to the downstream detection time. This method removed those ensemble members that were not detected at both locations and eliminated the randomness acquired in the passage downstream. Although more sophisticated techniques can be used, this simple method was sufficient to indicate the strength of the Reynolds stress downstream. The results are shown in figure 15 as the lowermost trace with the time shift taken as the average delay of those members in the ensemble average. As can be seen, most of the Reynolds shear stress is still evident although the decay is evident.

This technique was also applied to the data shown in figure 11 in order to eliminate the effects of the random convection velocity. In this case, the detection criterion was reapplied downstream to the data obtained at  $y^+ = 15$ . Then, if the above time-difference criterion was satisfied, the data were added to the

ensemble average. The results yielded a much sharper acceleration below  $y^+ = 25$  than that shown in figure 11 and a broad momentum excess persisted in the log region. However, the overall results were not changed as dramatically as those shown in figure 15. This is expected because the Reynolds stress will be more sensitive to the random phase associated with the variations in the convection velocity.

## 5. Discussion

The technique of conditional sampling will unfortunately have some degree of arbitrariness associated with it, primarily because of the choice of the detection criterion. In the outer intermittent region of the boundary layer, the choice of a detection function is relatively simple because the flow regime either does or does not contain vortical fluctuations. In the bursting phenomenon this sharp discrimination is not possible because of the inherent background turbulence. Hence conditionally averaged results in this region must be accepted with caution because, in a sense, they may represent only a part of the physical phenomenon which is occurring, as is discussed in more detail by Kaplan (1973) and also in the appendix. Having given fair warning about over-interpreting these results, we nevertheless do feel that the physical process identified is an important feature of the transport phenomenon in the wall region of a turbulent boundary layer, and not a feature of our detection criterion as demonstrated in §3.4.

The first justification for this conclusion is that the same process has been identified by many observers using widely different techniques. The present results use a detector function which is triggered by local rapid changes, and demonstrate an identifiable sequence of states associated with these events.

The size and rapidity with which the conditional averages grow are another indication of their importance. The amplitude of the event and the ease of recognizing its distinctive form indicate that a small signal is not being educted from a noisy environment, but that it is an identifiable and significant part of the turbulence. Additionally, the size of the spatial coherence of the structure is of interest, as well as the duration of its distinctive signature as it is convected downstream, once the influence of random convective motion is understood and correctly interpreted.

Finally, the high content of Reynolds shear stress during the bursting process is of interest, for these events apparently are the most important contributors to the long-time average of the Reynolds stress. The intermittent nature of the  $uv$  product appears to be intimately related to these structures.

Several other conclusions can be reached. Although the effect is largest near the wall, and its vertical extent scales with the sublayer co-ordinates  $v$  and  $u^*$ , its frequency of occurrence scales with the outer variables  $\delta$  and  $U_\infty$ . While the measurements cannot determine causal relationships without ambiguity, the existence of a sequence earlier in time than the burst suggests that the phenomenon is primarily driven by the outer turbulence. However, the relatively coherent nature of the averages downstream of and above the 'burst' leads one

to conclude that it may be driving the outer turbulence. Hence the burst is part of the complex process by which the turbulence in the boundary layer can regenerate itself.

No direct connexion between the large-scale outer movement of the interface between turbulent and non-turbulent fluid and an individual burst has been found. It is unreasonable to expect a one-to-one relationship between these two phenomena because of the differences in size and the degree of interaction between the newly generated turbulence and the old turbulence that exists in the boundary layer. It would be theoretically interesting to investigate the consequences of such a relationship for it could conceivably provide an additional link between the eddy-viscosity and entrainment models of the structure of turbulent shear layers.

It is felt that any future work in this area will have to study the effect of the random phase between the position of the detector and the sampling location. This randomness may be due to an unsteady convection velocity, random angles associated with the eddy in different planes, non-uniform trajectories of the eddies, etc. This unknown parameter will become more important as one attempts to sample data at increasing distances from the point of detection. Similarly, this phenomenon will make it more difficult to establish the cause-and-effect relationship between the bursts and the outer flow field, although a recent thesis by Chen (1975) illustrates one possible means by which this problem may be approached. However, future endeavours in this area may have to gather information from additional locations in space or make better use of existing information.

We gratefully acknowledge the fruitful discussions with our colleagues Dr John Laufer and Dr F. K. Browand. Our thanks to Mr George Tennant for the construction of the hot-wire rake. We also wish to thank Lindy A. Harper and Elizabeth C. Harris for typing the manuscript. This research was supported by the U.S. Army under grant DA-ARO-D-31-124-73-G118 and by the National Science Foundation under grant GK 35800X.

## Appendix

As with any detection scheme, the dependence of the conditionally averaged results on the threshold level is of obvious importance. Clearly, one desires to define a criterion such that the results are independent of the threshold value. Figure 6 shows that, although there is clearly an eddy structure associated with the detection scheme, the values do depend slightly on the threshold value  $k$  used in the detection scheme.

This dependence is not altogether surprising when one considers that not all of the deterministic eddies will have the same amplitude, but that, in fact, a distribution of amplitudes and sizes will probably prevail. This amplitude randomness will be augmented by the three-dimensionality of the eddy. A non-uniform amplitude was included by Rice (1944) in his discussion of a random signal generated by a deterministic process.

The definition of the detection criterion used here was dependent upon the

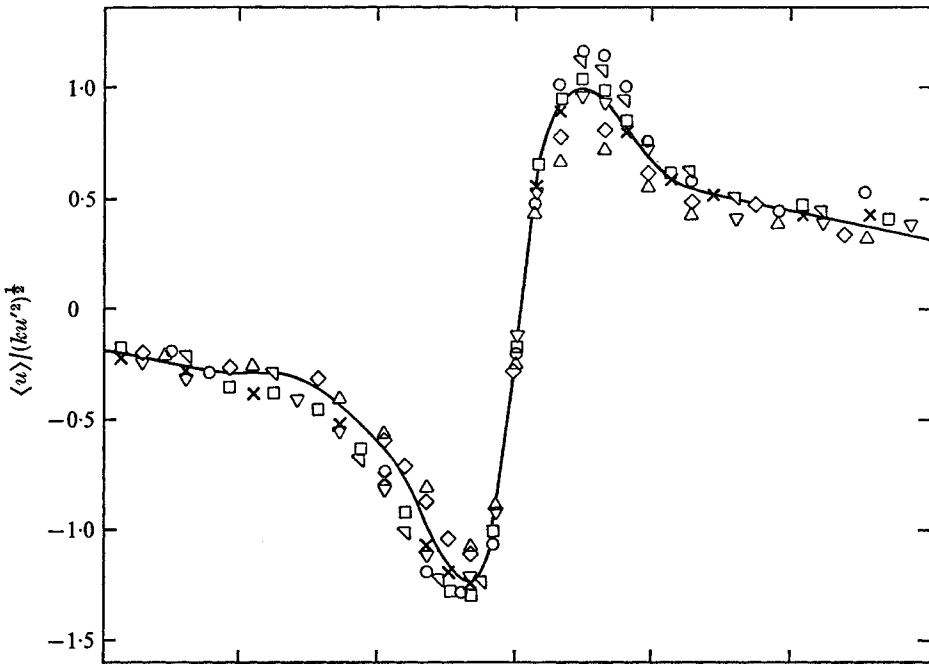


FIGURE 16. Conditional average of streamwise velocity component at  $y^+ = 15$  with various threshold levels.

	$\triangle$	$\diamond$	—	$\square$	$\times$	$\nabla$	$\circ$
$k$	0.9	1.0	1.2	1.4	1.6	1.8	2.5

threshold value  $ku'^2$ . Thus, as  $k$  is increased, one would expect that only the more intense events would be detected and the conditional averages would be correspondingly larger. This, indeed, was observed to be correct. However, if the eddy structure under study is truly deterministic, then the conditional averages at different threshold levels should scale monotonically with the threshold value.

This was verified by studying the data used to obtain figure 10. The conditional averages were obtained using threshold values from 0.9 to 2.5. It was found that the amplitude of the results varied by at most a factor of two when normalized with  $(u'^2)^{1/2}$ . However, when the data were normalized with the threshold r.m.s. of  $(ku'^2)^{1/2}$ , the results collapsed onto a single curve.

An example of this is shown in figure 16 for  $y^+ = 15$ . Even though the detection and sampling took place at the same location, the collapse was similar when these locations did not coincide. Thus the variation of the threshold parameter over this range affects only the magnitude of the detected event, and not its structure. Since the threshold value used throughout the remaining portion of this work was 1.2, the effect of this scaling was small, and thus neglected.

It should be mentioned that the same scaling effect was observed for even higher values of the threshold, although for  $k > 2.5$  relatively few events were detected. Thus considerably longer time records were required in order to obtain smooth averages. However, for threshold values less than 0.9, the above scaling

did not collapse the data onto a single curve. This was expected because at these lower values a significant percentage of the detected events were rapid decelerations instead of accelerations. The inclusion of these events in the ensemble average tends to decrease sharply the amplitude of the averages because of the diverse nature of these two structures.

## REFERENCES

- BAKEWELL, P. & LUMLEY, J. L. 1967 *Phys. Fluids*, **10**, 1880.
- BLACKWELDER, R. F. & KAPLAN, R. E. 1972 Intermittent structures in turbulent boundary layers. *NATO-AGARD Conf. Proc.* no. 93. London: Technical Editing & Reproduction Ltd.
- BRODKEY, R. S., WALLACE, J. M. & ECKELMANN, H. 1974 *J. Fluid Mech.* **63**, 209.
- CHAMPAGNE, F. H., HARRIS, V. G. & CORRSIN, S. C. 1970 *J. Fluid Mech.* **41**, 81.
- CHEN, C. H. P. 1975 The large scale motion in a turbulent boundary layer: a study using temperature contamination. Ph.D. thesis, University of Southern California, Los Angeles.
- CORINO, E. R. & BRODKEY, R. S. 1969 *J. Fluid Mech.* **37**, 1.
- CORRSIN, S. 1957 *Proc. 1st Naval Hydr. Symp.*, p. 373. Pub. SIS, Nat. Acad. Sci./Nat. Res. Council.
- EMMERLING, R. 1973 Die Momentane Struktur des Wanddruckes einer turbulenten Grenzschichtströmung. *Mitt. MPI Stromungsforsch u. Aerodyn. Versuchsanst., Göttingen*, no. 56.
- GRASS, A. J. 1971 *J. Fluid Mech.* **50**, 233.
- GUPTA, A. K., LAUFER, J. & KAPLAN, R. E. 1971 *J. Fluid Mech.* **50**, 493.
- KAPLAN, R. E. 1973 *Proc. Symp. Turbulence in Liquids*. University of Missouri Press.
- KAPLAN, R. E. & LAUFER, J. 1969 *Proc. 12th Int. Cong. Appl. Mech., Stanford*, p. 236. Springer.
- KIM, H. T., KLINE, S. J. & REYNOLDS, W. C. 1971 *J. Fluid Mech.* **50**, 133.
- KLINE, S. J., REYNOLDS, W. C., SCHRAUB, F. A. & RUNSTADLER, P. W. 1967 *J. Fluid Mech.* **30**, 741.
- KOVASZNAY, L. S. G., KIBENS, V. & BLACKWELDER, R. 1970 *J. Fluid Mech.* **41**, 283.
- LAUFER, J. & BADRI NARAYANAN, M. A. 1971 *Phys. Fluids*, **14**, 182.
- LU, S. S. & WILLMARTH, W. W. 1973a *Phys. Fluids*, **16**, 2012.
- LU, S. S. & WILLMARTH, W. W. 1973b *J. Fluid Mech.* **60**, 481.
- LUMLEY, J. L. 1970 *Stochastics Tools in Turbulence*. Academic.
- NARAHARI RAO, K., NARASIMHA, R. & BADRI NARAYANAN, M. A. 1971 *J. Fluid Mech.* **48**, 339.
- OFFEN, G. & KLINE, S. J. 1973 *Stanford University Mech. Engng Dept. Rep.* MD-31.
- RICE, S. O. 1944 *Bell System Tech. J.* **23**, 282.
- WALLACE, J. M., ECKELMANN, H. & BRODKEY, R. S. 1972 *J. Fluid Mech.* **54**, 39.
- WILLMARTH, W. W. & LU, S. S. 1972 Structure of Reynolds stress near the wall. *NATO-AGARD Conf. Proc.* no. 93. London: Technical Editing & Reproduction Ltd.

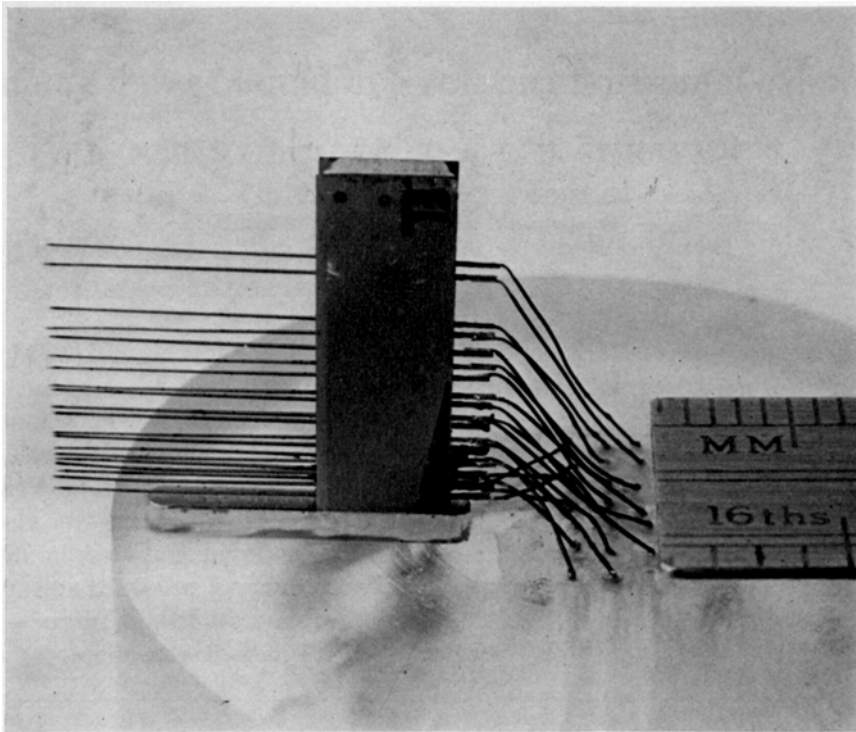


FIGURE 1. Photograph of the ten-wire rake used for measuring the instantaneous streamwise velocities at different positions in the normal direction.

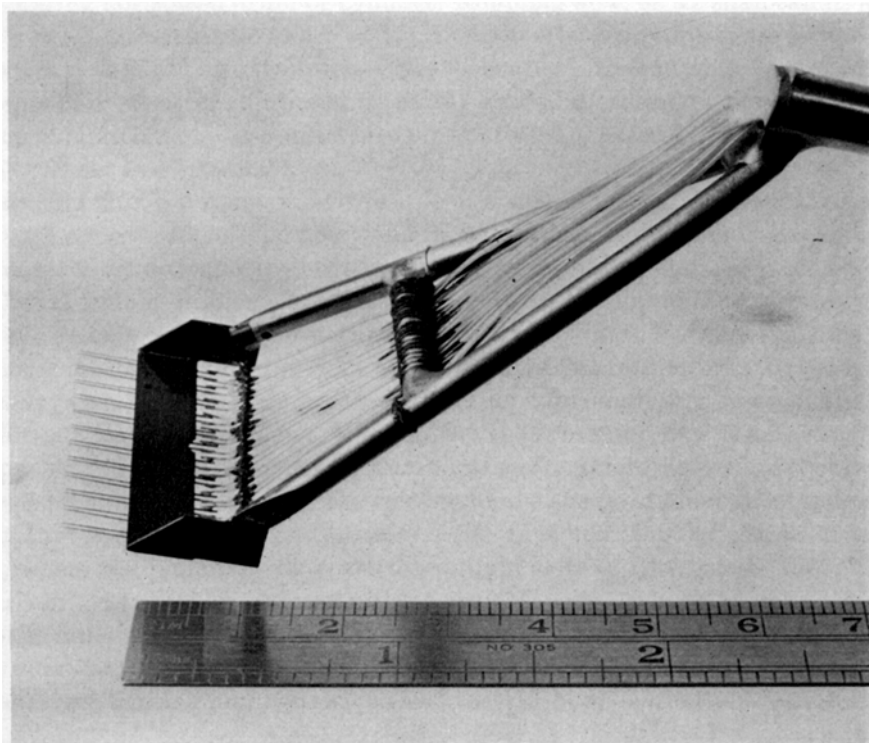


FIGURE 2. Photograph of the rake used for measuring the instantaneous streamwise velocities at 12 different positions in the spanwise direction.

